Eur. Phys. J. Spec. Top. (2026) 235:7265–7281
https://doi.org/10.1140/epjs/s11734-025-02059-z

THE EUROPEAN PHYSICAL JOURNAL SPECIAL TOPICS

Regular Article

Pattern characterization in non-locally coupled chaotic systems

C. A. S. Batista[1], A. S. Bispo[2], and R. L. Viana[2,3,a]

[1] Centro de Estudos do Mar, Universidade Federal do Paraná, 83255-976 Pontal do Paraná, Paraná, Brazil
[2] Departamento de Física, Universidade Federal do Paraná, 81531-980 Curitiba, Paraná, Brazil
[3] Centro Interdisciplinar de Ciência, Tecnologia e Inovação, Núcleo de Modelagem e Computação Científica, Universidade Federal do Paraná, Curitiba, Paraná, Brazil

Received 25 May 2025 / Accepted 3 November 2025 / Published online 9 November 2025
© The Author(s), under exclusive licence to EDP Sciences, Springer-Verlag GmbH Germany, part of Springer Nature 2025

Abstract We consider a model for a non-local coupling of chaotic systems, in which the interaction among them is mediated by the local concentration of a substance which diffuses along the spatial medium in which the systems are embedded. We assume that the diffusion time is vanishingly small, such that the concentration of the chemical reaches immediately its equilibrium limit. The Green function for the diffusion problem, with absorbing boundary conditions, is obtained for three geometries: bounded linear, rectangular, and circular domains. The resulting system of coupled differential equations was numerically integrated in the case that the chaotic systems are given by Rössler equations. The snapshots, or spatial patterns at fixed time, were analyzed using diagnostics of spatial coherence, such as a local order parameter based on a geometrical phase defined for each system. We analyzed the formation of chimera states, or inhomogeneous spatial patterns presenting both coherent and incoherent regions, for the three geometries considered and studied the dependence of results with the coupling parameters.

1 Introduction

Several problems of physical and biological interest involve pointlike dynamical systems ("cells") with an interaction mediated by a substance which is both secreted and absorbed by the cells, and diffuses along the medium in which the cells are embedded [1]. The coupling among systems is thus non-local, since it involves all the cells, and the coupling strength decreases with the distance among oscillators. The fast-relaxation limit of this model was proposed by Kuramoto, for which the dynamics of each system influences the production of a chemical substance obeying a diffusion equation, and the absorption depends on the local concentration of this substance at each cell position [2].

Since its introduction, the Kuramoto model of chemical coupling has been intensively studied, in the description of various phenomena such as power-law spatial correlations [3], chimeras [4], Turing–Hopf mixed mode solutions [5], noisy on–off intermittency with multi-scaling properties [6], noise-induced transition to turbulence [7], and phase turbulence [8]. This model, in particular, has many biological applications, such as neuronal networks of coupled Hodgkin–Huxley equations with excitatory and inhibitory coupling [9], the transition to bursting synchronization in neuronal networks [10], and the interaction among biological clock cells of the suprachiasmatic nucleus [11]. In the latter, the synchronization of clock cells is due to their interaction mediated by a neurotransmitter [12, 13]. The transition to synchronization of networks of phase oscillators with chemical coupling has been investigated both numerically [14] and analytically [15].

In the Kuramoto model of chemical coupling, it is assumed that the diffusion characteristic time is much shorter than the oscillator main period, such that diffusion is so fast that the system achieves instantaneously a stationary concentration of the diffusing chemical [2]. Recently, a generalization of this model was proposed for situations, where the characteristic diffusion time is comparable or even larger than the oscillator period [16]. There results a coupled system of integro-differential equations, which can be computationally solved by an approximation method

[a] e-mail: viana@fisica.ufpr.br (corresponding author)

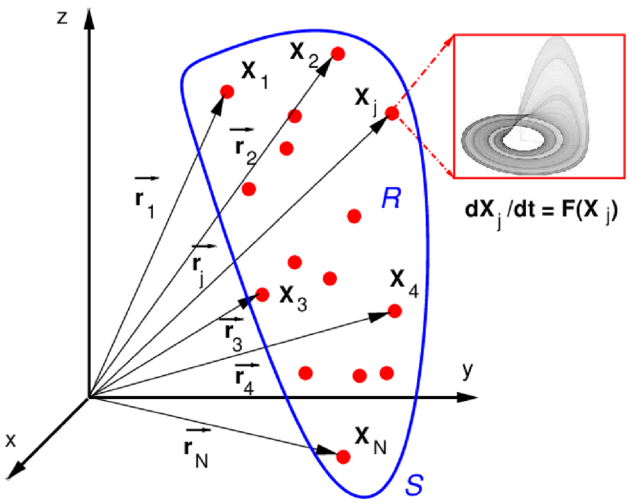


Fig. 1 System of pointlike chaotic Rössler systems

[16], or also by a fully numerical scheme,, which requires the knowledge of all the previous history of each system to advance the solution by one timestep [17].

The computational difficulties related to the latter procedure (and the corresponding CPU time) are much less than those existing for the fast-relaxation case. On the other hand, in the Kuramoto model of chemical coupling, only Green's functions for free space have been given [6]. In the present work, we present Green's functions for the Kuramoto model in bounded domains, in one and two spatial dimensions. These Green's functions are then used in the coupled system of ordinary differential equations describing the dynamics of the system. We considered an assembly of chaotic dynamical systems described by Rössler equations [18], in one-dimensional bounded intervals, and rectangular and circular domains in two dimensions.

The spatio-temporal dynamics exhibited by the numerical solutions we obtained is focused on chimera patterns presenting both spatially coherent and incoherent domains. Although a wide variety of examples of chimeras have been proposed *avant la lettre* [19–24], the word chimera was later introduced by Abrams and Strogatz [25]. Chimeras have been observed not just in numerical simulations of dynamical systems, but also in experiments, such as electrochemical oscillations [26], Josephson junction networks [27], delayed-feedback electronic systems [28], liquid-crystal spatial light modulators [29], and coupled Belousov–Zhabotinsky chemical oscillators [30].

It is possible to characterize the presence of chimera patterns using a quantifier based on a local order parameter [31, 32]. The latter was used in a system of coupled logistic maps and Rössler equations, where the coupling has finite reach [32]. A similar analysis considered coupled logistic maps when the coupling decays with the lattice distance as a power law [33].

In this work, we aim to investigate chimera patterns at fixed time for a network of Rössler systems (in a chaotic regime) with a coupling mediated by the diffusion of a chemical. We start from the general model of finite diffusion time and consider the adiabatic (fast relaxation) limit, for which the diffusion time is vanishingly small. As a consequence, the concentration of the diffusing chemical immediately reaches its equilibrium value, and the original system of integro-differential equations reduces to a much more manageable system of coupled ordinary differential equations, which are numerically solved. The local order parameter is used to characterize the presence of chimera patterns, where coherent and incoherent states coexist. This diagnostic is used to investigate the dependence on the coupling parameters, namely, the coupling strength, the degradation coefficient, and the diffusion coefficient of the chemical.

This paper is organized as follows: in Sect. II, we present the coupling model based on the solution of a reaction–diffusion equation governing the interaction among cell oscillators. In Sect. III, we show the Green's functions in free space in one, two, and three dimensions. The case of finite domains is considered in Sect. IV. Section V presents a system of coupled chaotic systems, and the characterization of chimera patterns. Our conclusions are left to the final section.

2 Coupling model

In this section, we present the general formulation of a mathematical model for chemically coupled dynamical systems. We deal with two classes of vectors: (i) positions $\mathbf{r}$ in a d-dimensional Euclidean space in which the systems are embedded; (ii) state variables $\mathbf{X} = (X_1, X_2, \ldots X_M)^T$ in an M-dimensional phase space of the dynamical variables characterizing the state of the system at a given time t (Fig. 1). There are N pointlike systems located at discrete positions $\mathbf{r}_j$, where $j = 1, 2, \cdots N$, in the d-dimensional Euclidean space; and $\mathbf{X}_j$ is the state variable for each system, whose time evolution is governed by the autonomous vector field $\mathbf{F}(\mathbf{X}_j)$.

We suppose that the time evolution of each system is affected by the local concentration of a chemical, denoted as $A(\mathbf{r}, t)$, in the form

$$\frac{d\mathbf{X}_j}{dt} = \mathbf{F}(\mathbf{X}_j) + \varepsilon\, A(\mathbf{r}_j, t), \qquad (j = 1, 2, \ldots N), \tag{1}$$

where $\mathbf{X}_j = \mathbf{X}(\mathbf{r} = \mathbf{r}_j, t)$ and $\varepsilon > 0$ stand for the intensity of the coupling. In the following, we suppose that all variables, including spatial coordinates and time, are non-dimensional.

The chemical concentration satisfies a diffusion equation of the form

$$\frac{\partial A(\mathbf{r}, t)}{\partial t} + \eta\, A(\mathbf{r}, t) - D\, \nabla^2 A(\mathbf{r}, t) = \sum_{k=1}^{N} h(\mathbf{X}_k(t))\, \delta(\mathbf{r} - \mathbf{r}_k), \tag{2}$$

where η is a phenomenological damping parameter (representing the chemical degradation of the mediating substance) and D is a diffusion coefficient. The diffusion equation has a source term h which depends on the system state at the discrete positions $\mathbf{r}_j$ of the systems, i.e., each "cell" is meant to produce the chemical with a rate depending on the current value of its own state variable.

To solve the non-homogeneous diffusion equation (2) we consider a bounded domain $\mathcal{R}$, where there is a surface $\mathcal{S}$ on which we specify suitable boundary conditions. One such example is absorbing (homogeneous Dirichlet) boundary conditions, for which the concentration vanishes on $\mathcal{S}$, i.e., $A(\mathbf{r} \in \mathcal{S}, t) = 0$. Moreover, we must specify the initial conditions along $\mathcal{R}$. For simplicity, we suppose that initially there is no substance in the domain: $A(\mathbf{r} \in \mathcal{R}, t = 0) = 0$.

The Green function for Eq. (2), denoted by $G(\mathbf{r}, t|\mathbf{r}', t')$, satisfies

$$\frac{\partial G}{\partial t} + \eta G - D\, \nabla^2 G = \delta(\mathbf{r} - \mathbf{r}')\, \delta(t - t'), \tag{3}$$

with the following boundary and initial conditions, respectively

$$G(\mathbf{r} \in \mathcal{S}, t|\mathbf{r}', t') = 0, \qquad G(\mathbf{r}, t = 0|\mathbf{r}'; t') = 0, \tag{4}$$

as well as the causality condition $G(\mathbf{r}, t|\mathbf{r}'; t') = 0$, if $t < t'$. It follows that the Green's function has the symmetry property

$$G(\mathbf{r}, t|\mathbf{r}', t') = G(\mathbf{r}', -t'|\mathbf{r}, -t).$$

On multiplying (2) by $G(\mathbf{r}, t|\mathbf{r}', t')$ and (3) by $A(\mathbf{r}', t')$, then subtracting the expression and integrating over primed volume and primed time t', we obtain a solution to the non-homogeneous diffusion equation for absorbing boundary conditions and vanishing initial concentration

$$A(\mathbf{r}, t) = \sum_{k=1}^{N} \int_0^{t^+} dt'\, h(\mathbf{X}_k(t'))\, G(\mathbf{r}, t|\mathbf{r}_k, t'). \tag{5}$$

Inserting this expression into Eq. (6) gives a system of integro-differential equations for the dynamical variables $\mathbf{X}_j(t)$:

$$\frac{d\mathbf{X}_j}{dt} = \mathbf{F}(\mathbf{X}_j) + \varepsilon \sum_{k=1}^{N} \int_0^{t^+} dt'\, h(\mathbf{X}_k(t'))\, G(\mathbf{r}_j, t|\mathbf{r}_k, t'), \qquad (j = 1, 2, \ldots N), \tag{6}$$

where the coupling term depends not only on the current system state, but also on all its history over time.

We can further simplify the model by assuming that the diffusion is so fast, compared with the characteristic timescale T of the systems, that we may set $\dot{A} \approx 0$, such that the concentration relaxes to a stationary value (adiabatic limit) [2–4]. The adiabatic limit can be taken if the diffusion time τ_c is much less than T. Let ℓ be the characteristic length of the system: from the diffusion equation (2) we can estimate the diffusion time as

$$\tau_c \sim \left(\frac{D}{\ell^2} - \eta\right)^{-1}, \tag{7}$$

such that the adiabatic limit is valid inasmuch as the diffusion coefficient satisfies the condition $D \ll \ell^2(\eta + 1/T)$.

3 Green functions in the free space

We begin by the simplest case in which there are no bounding surfaces, i.e., the domain is the entire space (this is equivalent to making the surface $\mathcal{S}$ "going to infinity"), where the boundary condition is $A(|\mathbf{r}|\to\infty, t) = 0$. The Green function of the diffusion problem in the d-dimensional free space is obtained by solving (3) using Fourier transforms, and reads

$$G_d(\mathbf{r}, t|\mathbf{r}_k, t') = \frac{\Theta(t-t')\, e^{-\eta(t-t')}}{(2\pi)^d} \int d^d\mathbf{k}\, e^{i\,\mathbf{k}\cdot(\mathbf{r}-\mathbf{r}_k) - D\,k^2(t-t')}, \tag{8}$$

where Θ is the Heaviside unit-step function. For one, two, and three dimensions, the Green function (8) is given, respectively, by [34]

$$G_1(x, t|x_k, t') = \frac{\Theta(t-t')\, e^{-\eta(t-t')}}{\sqrt{4\pi D\,(t-t')}} \exp\left[-\frac{(x-x_k)^2}{4\,D(t-t')}\right], \tag{9}$$

$$G_2(\mathbf{r}, t|\mathbf{r}_k, t') = \frac{\Theta(t-t')\, e^{-\eta(t-t')}}{4\pi D(t-t')} \exp\left[-\frac{(x-x_k)^2 + (y-y_k)^2}{4\,D\,(t-t')}\right], \tag{10}$$

$$G_3(\mathbf{r}, t|\mathbf{r}_k, t') = \frac{\Theta(t-t')\, e^{-\eta(t-t')}}{[4\pi D(t-t')]^{3/2}} \exp\left[-\frac{(x-x_k)^2 + (y-y_k)^2 + (z-z_k)^2}{4\,D\,(t-t')}\right]. \tag{11}$$

It is useful to define an interaction kernel as the time integral of the Green function, as

$$\sigma_d(\mathbf{r}, \mathbf{r}_k; t) = \int_0^{t^+} dt'\, G_d(\mathbf{r}, t|\mathbf{r}_k, t'), \tag{12}$$

such that, for the one-dimensional case, it is given by

$$\sigma_1(x, x_k, t) = \int_0^{t^+} dt'\, \frac{e^{-\eta\,(t-t')}}{\sqrt{4\pi D\,(t-t')}} \exp\left[-\frac{(x-x_k)^2}{4\,D\,(t-t')}\right], \tag{13}$$

which becomes, after a change of variables

$$\sigma_1(x, x_k, t) = \frac{x-x_k}{4\,D\sqrt{\pi}} \int_{u_1}^{\infty} du\, \frac{e^{-u-a_1/u}}{u^{3/2}}, \tag{14}$$

where

$$a_1 = \frac{\eta(x-x_k)^2}{4\,D} = \left\{\frac{\gamma(x-x_k)}{2}\right\}^2, \qquad u_1 = \frac{(x-x_k)^2}{4\,D\,t}, \tag{15}$$

and we defined a coupling length

$$\gamma = \sqrt{\frac{\eta}{D}}. \tag{16}$$

For the two-dimensional case, the interaction kernel is

$$\sigma_2(\mathbf{r},\, \mathbf{r}_k; t) = \frac{1}{4\,\pi\,D}\int_{u_2}^{\infty} \frac{du}{u}\, e^{-u-a_2/u}, \tag{17}$$

where

$$a_2 = \frac{\eta[(x-x_k)^2 + (y-y_k)^2]}{4\,D} = \left|\frac{\gamma(\mathbf{r}-\mathbf{r}_k)}{2}\right|^2, \qquad u_2 = \frac{|\mathbf{r}-\mathbf{r}_k|^2}{4\,D\,t}, \tag{18}$$

and, similarly, the kernel in three dimensions is

$$\sigma_3(\mathbf{r},\, \mathbf{r}_k; t) = -\frac{1}{4\,D\,\pi^{3/2}}\frac{1}{|\mathbf{r}-\mathbf{r}_k|}\int_{u_3}^{\infty} \frac{du}{\sqrt{u}}\, \exp\Big(-u - \frac{a_3}{u}\Big), \tag{19}$$

where

$$a_3 = \frac{\eta}{4\,D}|\mathbf{r}-\mathbf{r}_k|^2, \qquad u_3 = \frac{|\mathbf{r}-\mathbf{r}_k|^2}{4\,D\,t}. \tag{20}$$

Now we consider the adiabatic limit (7), for which we can suppose that the diffusion is practically instantaneous, i.e., the chemical concentration relaxes immediately to its equilibrium value $\dot{A}_E = 0$. In this limit, the diffusion equation no longer involves the time explicitly

$$\eta\, A_E(\mathbf{r}) - D\,\nabla^2 A_E(\mathbf{r}) = \sum_{k=1}^{N} h(\mathbf{X}_k)\,\delta(\mathbf{r}-\mathbf{r}_k), \tag{21}$$

such that the equilibrium concentration, with the same boundary and initial conditions of the time-dependent case, is given by

$$A_E(\mathbf{r}) = \sum_{k=1}^{N} h(\mathbf{X}_k)\, G_E(\mathbf{r}|\mathbf{r}_k), \tag{22}$$

where the equilibrium Green function is a solution of

$$\eta\, G_E - D\,\nabla^2 G_E = \delta(\mathbf{r}-\mathbf{r}'). \tag{23}$$

The coupled system of equations, in the adiabatic (equilibrium) limit, is obtained by substituting (22) into (21), and reads

$$\left.\frac{d\mathbf{X}_j}{dt}\right|_E = \mathbf{F}(\mathbf{X}_j) + \varepsilon \sum_{k=1}^{N} h(\mathbf{X}_k)\, G_E(\mathbf{r}_j|\mathbf{r}_k). \tag{24}$$

Since the coupling term depends only on the current value of the dynamical variables, (24) is a system of coupled differential equations, much simpler to solve than the integro-differential case (6). Comparing both sets of equations, (6) reduces to (24) if: (i) the source function $h(.)$ does not involve time explicitly; (ii) the equilibrium Green function is the infinite-time limit of the interaction kernel (12):

$$G_{Ed}(\mathbf{r}_j|\mathbf{r}_k) = \lim_{t\to\infty} \sigma_d(\mathbf{r}_j,\, \mathbf{r}_k; t). \tag{25}$$

If we take this limit on the one-dimensional interaction kernel given by Eq. (14) we obtain the following result:

$$G_{E1}(x_j|x_k) = \frac{\gamma}{2\,\eta}\, e^{-\gamma\,(x_j - x_k)}, \tag{26}$$

which agrees, up to a normalization factor, with the earlier results of Kuramoto and coworkers [2, 6], in their analysis of the fast-relaxation case. In two and three dimensions the same limits applied to Eqs. (17)–(19) yield

$$G_{E2}(\mathbf{r}_j|\mathbf{r}_k) = \frac{1}{2\,\pi\,D}\,\mathcal{K}_0[\gamma\,|\mathbf{r}_j - \mathbf{r}_k|], \tag{27}$$

$$G_{E3}(\mathbf{r}_j|\mathbf{r}_k) = \frac{1}{4\,\pi\,D}\,\frac{e^{-\gamma|\,\mathbf{r}_j - \mathbf{r}_k|}}{|\mathbf{r}_j - \mathbf{r}_k|}, \tag{28}$$

where $\mathcal{K}_0$ is the modified Bessel function of order zero. These expressions coincide with those previously given by Nakao [6] , for the fast relaxation case.

4 Green functions in finite domains

If we consider that diffusion occurs over a bounded spatial domain, there results a boundary value problem for the diffusion equation. Adopting absorbing boundary conditions, i.e., the concentration vanishes at the boundary surface $\mathcal{S}$, the solution of the non-homogeneous diffusion equation is given by (5). The Green functions can be expressed as bilinear series expansions of orthogonal eigenfunctions of a self-adjoint operator [34]. The expansions depend on the geometry of the boundary as well as the dimension of the underlying space. Once the corresponding Green's function is obtained, the coupled system of integro-differential equations is given by (6).

Let us begin by considering a one-dimensional finite domain of length L ($0 \le x \le L$) with absorbing boundary conditions ($A(0,\,t) = A(L,\,t) = 0$). The corresponding Dirichlet Green's function is (see [34], Eq. 4.2.21)

$$G_1(x,\,t|x',\,t') = \frac{2\,\Theta(t-t')}{L}\sum_{n=1}^{\infty}\sin\Big(\frac{n\,\pi\,x}{L}\Big)\,\sin\Big(\frac{n\,\pi\,x'}{L}\Big)\,\exp\Big\{-\Big[D\Big(\frac{n\,\pi}{L}\Big)^2 + \eta\Big](t-t')\Big\}. \tag{29}$$

The adiabatic limit corresponds, as in the previous section, to the $t \to \infty$ of the corresponding interaction kernel, giving the following equilibrium limit of the Green's function:

$$G_{E1}(x_j|x_k) = \frac{2}{L}\sum_{n=1}^{\infty}\Big\{D\Big(\frac{n\,\pi}{L}\Big)^2 + \eta\Big\}^{-1}\sin\Big(\frac{n\,\pi\,x_j}{L}\Big)\,\sin\Big(\frac{n\,\pi\,x_k}{L}\Big). \tag{30}$$

One example of a two-dimensional domain is a rectangle of sides a and b with absorbing boundary conditions: $A(x = a,\,0 \le y \le b) = A(0 \le x \le a,\,y = b) = 0$, for which the Green's function is

$$\begin{aligned} G_{2r}(x,\,y,\,t|x',\,y',\,t') = \frac{4\,\Theta(t-t')}{a\,b}\sum_{n=1}^{\infty}\sum_{m=1}^{\infty}\sin\Big(\frac{n\,\pi\,x}{a}\Big)\,\sin\Big(\frac{n\,\pi\,x'}{a}\Big)\,\sin\Big(\frac{m\,\pi\,y}{b}\Big)\times \\ \sin\Big(\frac{m\,\pi\,y'}{b}\Big)\,\exp\Big\{-\Big[D\Big(\frac{n^2}{a^2}+\frac{m^2}{b^2}\Big)\pi^2 + \eta\Big](t-t')\Big\}, \end{aligned} \tag{31}$$

with equilibrium (adiabatic) limit given by

$$\begin{aligned} G_{E2r}(x_j,\,y_j|x_k,\,y_k) = \frac{4}{a\,b}\sum_{n=1}^{\infty}\sum_{m=1}^{\infty}\Big\{D\Big(\frac{n^2}{a^2}+\frac{m^2}{b^2}\Big)\pi^2 + \eta\Big\}^{-1}\times \\ \sin\Big(\frac{n\,\pi\,x_j}{a}\Big)\,\sin\Big(\frac{n\,\pi\,x_k}{a}\Big)\,\sin\Big(\frac{m\,\pi\,y_j}{b}\Big)\,\sin\Big(\frac{m\,\pi\,y_k}{b}\Big). \end{aligned} \tag{32}$$

Another example of a bounded two-dimensional domain is a circle of radius $r = a$ with an absorbing boundary ($A(r = a, \vartheta) = 0$). Using polar coordinates, the Green function is

$$G_{2c}(r, \vartheta, t|r', \vartheta', t') = \frac{\Theta(t-t')}{\pi a^2} \sum_{m=-\infty}^{\infty} \sum_{n=1}^{\infty} \frac{1}{[J'_m(x_{mn})]^2} J_m\left(x_{mn}\frac{r}{a}\right) J_m\left(x_{mn}\frac{r'}{a}\right) \times$$
$$\cos[m(\vartheta - \vartheta')] \exp\left\{-\left[\frac{D\, x_{mn}^2}{a^2} + \eta\right](t-t')\right\}, \tag{33}$$

where x_{mn} is the nth positive root of the Bessel function $J_m(x)$. Its equilibrium limit is

$$G_{E2c}(r_j, \vartheta_j|r_k, \vartheta_k) = \frac{1}{\pi a^2} \sum_{m=-\infty}^{\infty} \sum_{n=1}^{\infty} \left\{\frac{D\, x_{mn}^2}{a^2} + \eta\right\}^{-1} \cos[m(\vartheta_j - \vartheta_k)] \times$$
$$\frac{1}{[J'_m(x_{mn})]^2} J_m\left(x_{mn}\,\frac{r_j}{a}\right) J_m\left(x_{mn}\,\frac{r_k}{a}\right) \tag{34}$$

5 Systems of coupled Rössler equations

A linear coupling is given by $h(\mathbf{X}_k) = \mathbf{B}\mathbf{X}_k$, where $\mathbf{B}$ is a $M \times M$ matrix whose nonzero elements $B_{mn}^{(ij)}$ indicate that the mth variable of the jth oscillator is coupled to the nth variable of the kth oscillator. The future coupling, for which $h(\mathbf{X}_k) = \mathbf{B}\mathbf{F}(\mathbf{X}_k)$, is useful, because each oscillator remains in the same range as for the isolated system, in such a way that the state variables remain normalized. Moreover, the neighboring oscillators are evolved in time before they are coupled, providing a synchronous update for the coupled lattice at any time. Finally, a general nonlinear coupling can be represented as $h(\mathbf{X}_k) = \mathbf{B}\,\mathbf{H}(\mathbf{X}_k)$, and $\mathbf{H}$ is an arbitrary function of its arguments.

Let us consider the Rössler equations, for which $M = 3$ [18]

$$\mathbf{X}_j = \begin{pmatrix} X_j \\ Y_j \\ Z_j \end{pmatrix}, \qquad \mathbf{F}(\mathbf{X}_j) = \begin{pmatrix} -Y_j - Z_j \\ X_j + \tilde{a}\, Y_j \\ \tilde{b} + Z_j(X_j - \tilde{c}) \end{pmatrix}, \tag{35}$$

where $\tilde{a}$, $\tilde{b}$, and $\tilde{c}$ are system parameters. A chaotic attractor is known to exist for $\tilde{a} = \tilde{b} = 0.2$, and $\tilde{c} = 5.7$. From (6), a network of Rössler systems with linear coupling has the general form

$$\frac{dX_j}{dt} = -Y_j - Z_j +$$
$$\varepsilon \sum_{k=1}^{N} \int_0^t dt' \{B_{11}\, X_k(t') + B_{12}\, Y_k(t') + B_{13}\, Z_k(t')\}\, G(\mathbf{r}_j, t|\mathbf{r}_k, t'), \tag{36}$$
$$\frac{dY_j}{dt} = X_j + \tilde{a}\, Y_j +$$
$$\varepsilon \sum_{k=1}^{N} \int_0^t dt' \{B_{12}\, X_k(t') + B_{22}\, Y_k(t') + B_{23}\, Z_k(t')\}\, G(\mathbf{r}_j, t|\mathbf{r}_k, t'), \tag{37}$$
$$\frac{dZ_j}{dt} = \tilde{b} + Z_j(X_j - \tilde{c}) +$$
$$\varepsilon \sum_{k=1}^{N} \int_0^t dt' \{B_{31}\, X_k(t') + B_{32}\, Y_k(t') + B_{33}\, Z_k(t')\}\, G(\mathbf{r}_j, t|\mathbf{r}_k, t'), \tag{38}$$

where $j = 1, 2, \ldots N$. In the fast-relaxation limit, using (24), the equilibrium form of these equations (24) reads

$$\left.\frac{dX_j}{dt}\right|_E = -Y_j - Z_j + \varepsilon \sum_{k=1}^{N} (B_{11}\, X_k + B_{12}\, Y_k + B_{13}\, Z_k)\, G_E(\mathbf{r}_j|\mathbf{r}_k), \tag{39}$$

$$\left.\frac{dY_j}{dt}\right|_E = X_j + \tilde{a}\, Y_j + \varepsilon \sum_{k=1}^{N} (B_{12}\, X_k + B_{22}\, Y_k + B_{23}\, Z_k)\, G_E(\mathbf{r}_j|\mathbf{r}_k), \tag{40}$$

$$\left.\frac{dZ_j}{dt}\right|_E = \tilde{b} + Z_j(X_j - \tilde{c}) + \varepsilon \sum_{k=1}^{N} (B_{31}\, X_k + B_{32}\, Y_k + B_{33}\, Z_k)\, G_E(\mathbf{r}_j|\mathbf{r}_k), \tag{41}$$

where the equilibrium Green functions are to be used instead of the time-dependent ones.

To simplify the system, reducing the number of free parameters, we will choose $B_{11} = 1$ and all remaining matrix elements B_{jk} vanish. In such a way the Rössler equations, coupled through their X-variable, are

$$\frac{dX_j}{dt} = -Y_j - Z_j + \varepsilon \sum_{k=1}^{N} X_k\, G_E(\mathbf{r}_j|\mathbf{r}_k), \tag{42}$$

$$\frac{dY_j}{dt} = X_j + \tilde{a}\, Y_j \tag{43}$$

$$\frac{dZ_j}{dt} = \tilde{b} + Z_j(X_j - \tilde{c}) \tag{44}$$

where ε stands for the coupling strength, and we dropped the subscript E on the left-hand side for simplicity. The geometrical details of the spatial domain are contained in the corresponding equilibrium Green functions $G_E(\mathbf{r}_j|\mathbf{r}_k)$.

6 Spatial patterns and chimeras

There is a plethora of possible spatial patterns exhibited by coupled chaotic systems, many of them having been classified by Kaneko [35]: (i) frozen random patterns (chaotic behavior in spatial domains with boundaries fixed in time); (ii) pattern selection and suppression of chaos (domains of certain sizes are selected due to boundary motion); (iii) Brownian motion of defects and defect turbulence (diffusion of chaotic defects and intermittency due to pattern competition); (iv) fully developed turbulence.

More recently, a whole class of patterns has been called chimeras, defined as solutions that exhibit significantly different behavior in different regions of space or time. More specifically, chimeras refer to the coexistence between coherent and incoherent spatial domains. To characterize the degree of coherence exhibited by a chimera pattern, we have proposed a local order parameter based on a spatial phase. Let us consider a given snapshot spatial pattern $\{X_j\}$ (or any other state variable. We choose X, because the coupling term is applied directly on this variable rate).

We denote as $\max_j\{X_j\}$ and $\min_j\{X_j\}$ the maximum and minimum values of this snapshot pattern at fixed time t. A geometrical phase for the jth coupled system is defined by [31]

$$\sin\psi_j = \frac{2\, X_j - \max_j\{X_j\} - \max_j\{X_j\}}{\max_j\{X_j\} - \max_j\{X_j\}}, \qquad (j = 1,\, 2,\, \ldots N), \tag{45}$$

in such a way that a spatial half-cycle is mapped onto the phase interval $[-\pi/2,\, \pi/2]$. From this phase distribution along the network, a local order parameter magnitude is given by

$$R_j = \lim_{N\to\infty} \frac{1}{2\,\delta(N)} \left| \sum_{k\in C} \exp(i\,\psi_k) \right|, \qquad (j = 1,\, 2,\, \ldots N), \tag{46}$$

where C denotes a set of integers j and k such that $|j-k|/N \le \delta(N)$, where $\delta(N) \to 0$ if $N \to \infty$.

Within a coherent domain, the local order parameter magnitude takes on a value very close to unity, forming a plateau of sites with $R_j \approx 1$. This occurs, because the phasors corresponding to the phases ψ_j add coherently over a spatial distance. Incoherent regions, on the other hand, are such that their phases are distributed so as to have a smaller phasorial sum.

Given that plateaus with $R_j \approx 1$ correspond to coherent domains, a degree of coherence p was defined in Ref. [32] by computing the relative mean plateau size in a snapshot pattern. Let there be N_p coherence plateaus, each

of them with length N_j. The mean plateau size is $\bar{N} = (1/N_p)\sum_{j=1}^{N_p} N_j$. The coherence degree is defined as the ratio between the mean plateau size and the total lattice size, or $p = \bar{N}/N$.

If the entire pattern is coherent, i.e., if the order parameter magnitude is equal to unity for all sites, we have just one coherence plateau, such that $\bar{N} = N$ and $p = 1$. On the other hand, if we have a totally incoherent pattern, there would be as many plateaus as lattice sites, so $N_p \approx N$ and $\bar{N} \approx 1$, in such a way that $p = 1/N \to 0$ as $N \to \infty$. Chimeras, for which there are coherent regions separated by incoherent ones, are thus associated with $0 < p < 1$.

7 Numerical results

In this section, we consider networks of coupled Rössler systems exhibiting, when isolated, a chaotic attractor, for $\tilde{a} = \tilde{b} = 0.2$ and $\tilde{c} = 5.7$. The coupled set of equations for this case is obtained by substituting the corresponding Dirichlet Green function into Eqs. (42)–(44), according to the particular geometry taken into account. Three geometries will be considered in the present work: a one-dimensional (linear) domain of finite length, and two-dimensional domains (with rectangular and circular boundaries).

In each case, the system of coupled equations is numerically solved using a fourth-order Runge-Kutta method, with initial conditions given by

$$X_j(0) = 0.1\,\sin(\pi j), \qquad Y_j(0) = Z_j(0) = 0.1, \qquad (j = 1, 2, \ldots N).$$

The equations are evolved in time until $t_F = 2.1 \times 10^4$, and we considered snapshots of the lattice $\{X_j\}$ for a fixed time t_F. The corresponding Green functions involve simple or double summations of an infinite number of eigenfunctions. Since these summations converge very fast, it suffices to take five terms in each one for a good numerical convergence. Besides the coupling strength ε, we also have, for the coupling parameters, the diffusion coefficient D and the degradation coefficient η, both present in the equilibrium Green functions.

We first consider a linear domain of length L, wherein we orderly distribute N identical systems, each of them placed at discrete positions $x_j = j\Delta$, $(j = 1, 2, \ldots N)$, where $\Delta = L/(N+1)$. The equilibrium Green function for this case is given by (30) is inserted (42). For numerical purposes, we set $L = \pi$ and $N = 300$, such that $\Delta = \pi/301$. Figure 2 shows various snapshots (plots of $\{X_j\}$ *vs.* j at a fixed time t_F) corresponding to three different sequences of variable coupling parameters. Figure 2a–d shows for $D = \eta = 1.0$ and ε varying from zero

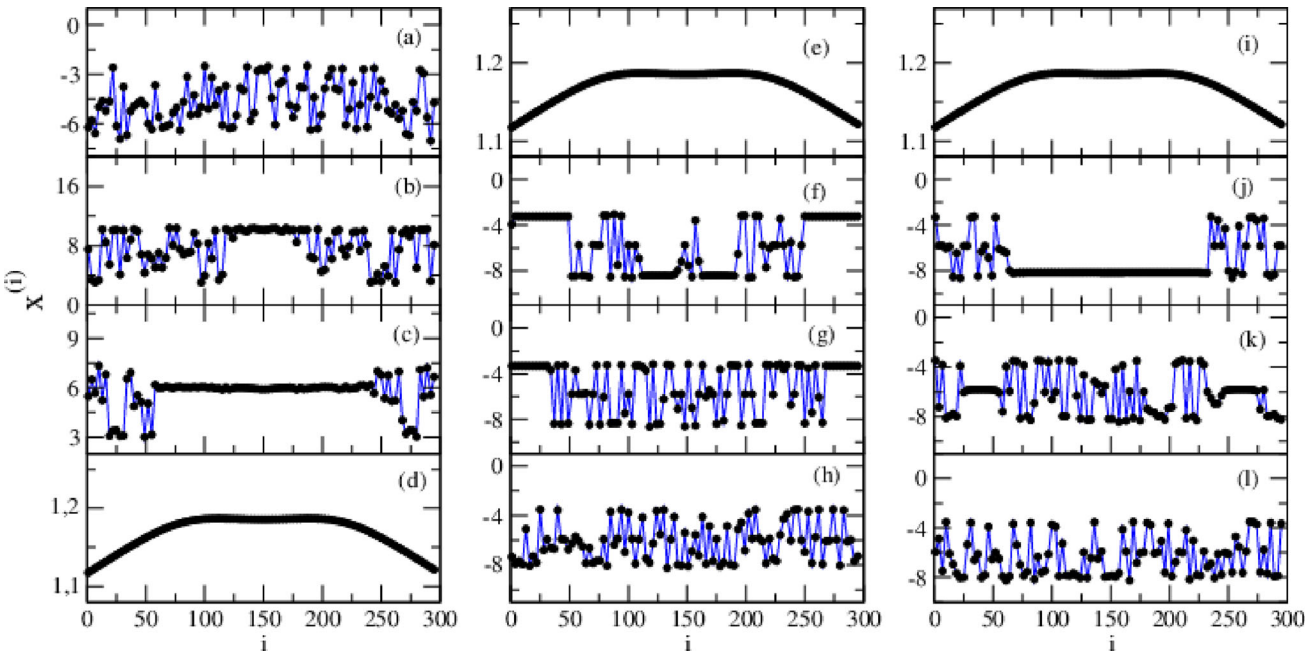


Fig. 2 Snapshot patterns for a lattice of $N = 300$ coupled identical Rössler systems at a fixed time t_F with coupling parameters: $D = \eta = 1.0$ and $\varepsilon =$ (a) 0.0, (b) 0.25, (c) 0.31, (d) 0.38; for $\varepsilon = 0.38$ and $\eta = 1.0$ and $D =$ (e) 1.0, (f) 1.3, (g) 1.4, (h) 2.0; for $\varepsilon = 0.38$, $D = 1.0$ and $\eta =$ (i) 1.0, (j) 1.8, (k) 2.9, (l) 3.2

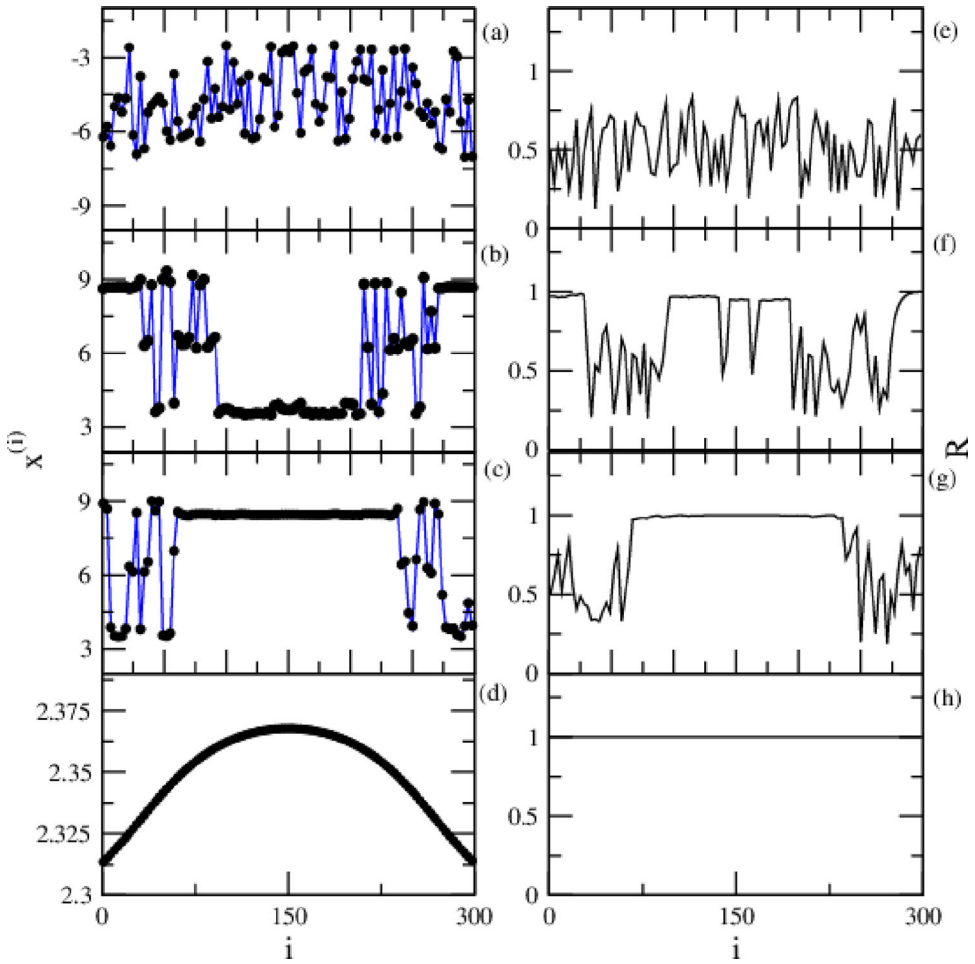


Fig. 3 Numerical results for a lattice of $N = 300$ coupled identical Rössler systems at a fixed time t_F. Left panels: snapshot patterns, right panels: order parameter magnitude spectrum for $D = \eta = 1.0$ and (a)–(e) $\varepsilon = 0.0$; (b)–(f) $\varepsilon = 0.271$; (c)–(g) $\varepsilon = 0.284$; (d)–(h) $\varepsilon = 0.38$

to 0.38. We observe the formation of chimera states for $\varepsilon = 0.25$ and 0.31. Conversely, such states disappear, as Fig. 2e–h illustrates, fixing $\varepsilon = 0.38$ and $\eta = 1.0$ and increasing D from 1.0 to 2.0. Another example (Fig. 2i–l) is for $\varepsilon = 0.38$ and $D = 1.0$ and increasing degradation coefficient.

The spectrum of order parameter magnitude values R_i, for $i = 1, 2, \ldots N$, is given in the right panels of Fig. 3, while in the left panels, we plot snapshots obtained for $D = \eta = 1.0$ and ε varying from zero to 0.38 (similar to Fig. 2a–d). For the totally incoherent pattern of Fig. 3a, the order parameter values are likewise irregularly distributed along the lattice, with values fluctuating around 0.5 (Fig. 3g). A chimera pattern is shown in Fig. 3b, where the coherent parts of the lattice correspond to some small plateaus in the order parameter spectrum (Fig. 3f). As ε increases further, the coherent region grows (Fig. 3c), as well as the plateau size (Fig. 3g), until we have a completely ordered pattern (Fig. 3d), with one plateau only (Fig. 3h).

In Fig. 4, we plot the degree of coherence p as a function of the coupling parameters for the linear domain case. Fixing $D = \eta = 1.0$ and varying ε we observe a transition from a totally incoherent state (small p) to a completely coherent one ($p \approx 1$), as ε increases past ~ 0.25 (Fig. 4a). Similar transitions have been described for synchronized states in coupled map lattices [32]. As a matter of fact, a synchronized state is an extreme example of a coherent pattern, with all the sites having the same values for their state variables. In lattices of phase oscillators, for example, this transition has been described theoretically by Kuramoto for global coupling [36]. Such transition was also observed in nonlocal couplings, where the interaction strength decreases with the lattice distance as a power law [37, 38]. Since the types of coupling described in this work are likewise nonlocal, such a transition to coherence is expected as the coupling strength increases.

On the other hand, the occurrence of this transition depends on the coupling parameter values. For example, it does not occur for $D = 2.0$ and $\eta = 3.0$ (Fig. 4b). An inverse transition, where the lattice starts completely coherent and turns totally incoherent, occurs for fixed $\varepsilon = 0.38$ and $D = 1.0$ and increasing η (Fig. 4c). The loss of coherence as the degradation coefficient increases has been previously described in a network of phase oscillators with chemical coupling, for which the full integro-differential equations have been solved [16]. In physical terms, the loss of coherence found as we increase the values of η can be understood by a reduction of the local concentration of the diffusing substance. Since the coupling effect depends on the latter, an increasing η means a weaker coupling

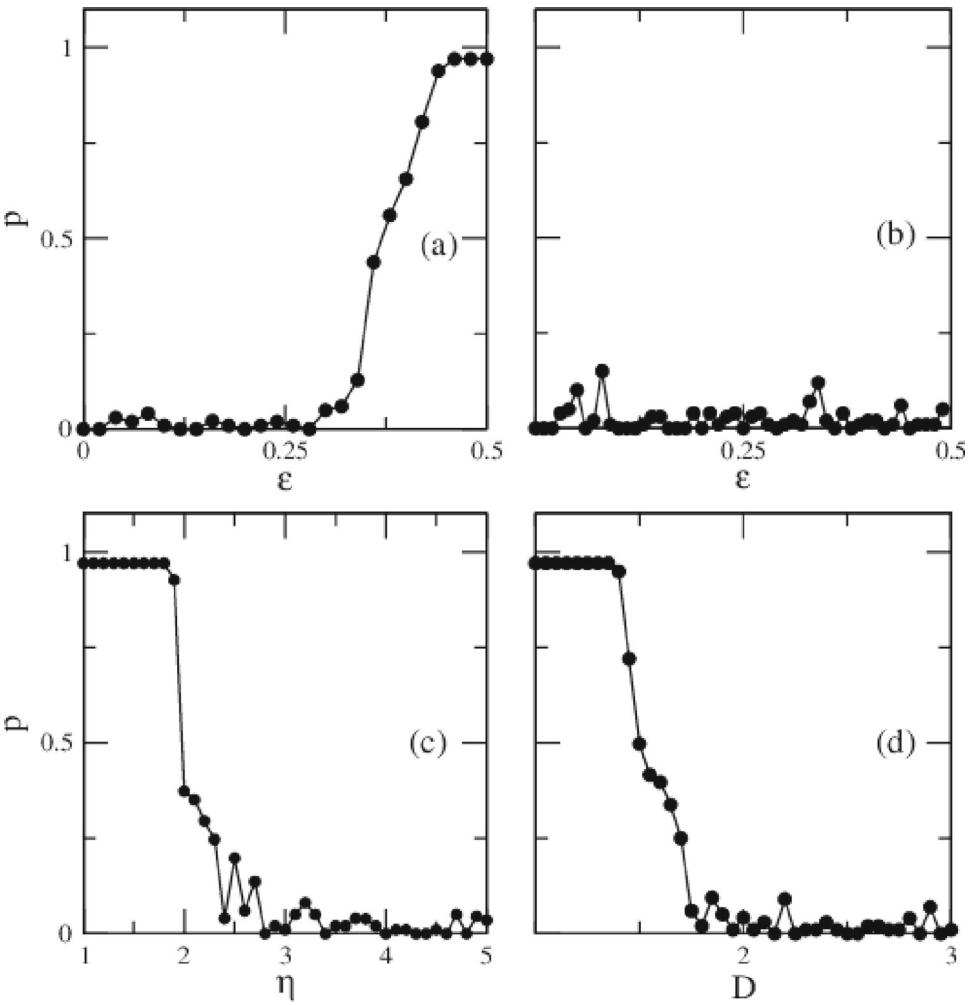


Fig. 4 Degree of coherence p as a function of (a) ε, for $D = \eta = 1.0$; (b) ε, for $D = 2.0$ and $\eta = 3.0$; (c) η, for $\varepsilon = 0.38$ and $D = 1.0$; (d) D, for $\varepsilon = 0.38$ and $\eta = 1.0$. The remaining parameter values are the same as in the previous figure

intensity, and thus a lesser degree of coherence for the lattice. The same behavior can be observed for fixed $\varepsilon = 0.38$ and $\eta = 1.0$ and varying diffusion coefficient D (Fig. 4d). The loss of coherence in this case is also explained by the local reduction of the chemical concentration when the diffusion is too strong, since the boundaries are absorbing.

Let us consider with more detail the transition to coherence observed for increasing ε, as illustrated in Fig. 4a. We can define a critical coupling strength ε_c as the value for which p is larger than a small tolerance (~ 0.08). In Fig. 4a, obtained for $N = 300$ coupled systems, this value is ~ 0.35, and we found that it decreases with the lattice size N. Figure 5 shows the values of ε_c as a function of $1/N$ for $D = \eta = 1.0$. As the lattice size N increases, the critical value tends to $\varepsilon_c \approx 0.328$.

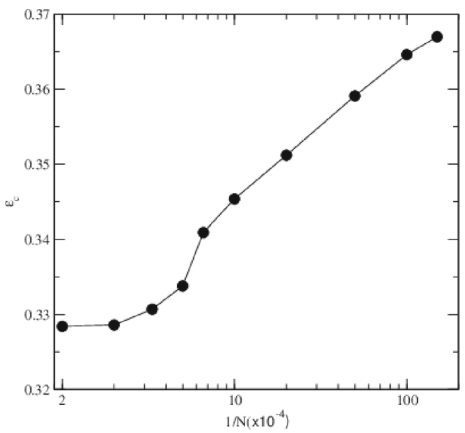


Fig. 5 Critical coupling strength as a function of the inverse lattice size for $D = \eta = 1.0$. The remaining parameter values are the same as in the previous figures

For a two-dimensional rectangular domain of sizes a and b, we define a square lattice with $M \times N$ identical systems placed at discrete positions $(x_i, y_j) = (\Delta_x i, \Delta_y j)$, $(i = 1, 2, \ldots M; j = 1, 2, \ldots N)$, where $\Delta_x = \Delta_y = a\,b/M\,N$. We numerically solved the coupled set of equations (42) with the corresponding equilibrium Green function given by (32), and choosing $a = 1$ and $b = 2$, $M \times N = 200$.

Cross sections of snapshot patterns, for this geometry, can be observed in Fig. 6. In the left panels, we plot snapshots of slices $\{X_{i,j}\}$ *vs.* i, j, where the i-sites (horizontal slice) are represented by blue lines and j-sites (vertical slice) by red lines, both at a fixed time t_F. From Fig. 6a, b, on increasing the coupling parameter, we observe that the oscillations start from a totally incoherent state, where $\varepsilon = 0$, there is the emergence of chimera patterns, as shown in Fig. 6b, c. Finally, for $\varepsilon = 0.38$ (Fig. 6d), the oscillation reaches completely coherent states, but the slices are different from each other for all cases. In the right panels (Fig. 6c–f), we plot the corresponding order parameter $R_{i,j}$.

Figure 7 displays the degree of coherence $p_{(i,j)}$ as a function of the coupling strength for the two-dimensional rectangular domain, where the blue line refers to the i-sites (horizontal slice) and the red line to the j-sites (vertical slice). We observe a transition from the completely incoherent state to coherent states at $\varepsilon \approx 0.36$, which appears more abrupt in comparison with the similar transition found in the linear domain case. We also plot (black line) the fraction $f = N_1/N$, where N is the total number of points on the plot and N_1 of points (i, j) for which $R \geq 0.95$. If $f = 1$ all points on the plot are coherent, if $f = 0$ none of the points are coherent. The result in the blue line shows the fraction f, which shows a similarity to the quantity p but, in this case, the transition occurs at $\varepsilon = 0.34$ and its maximum amplitude is slightly higher when compared to the degree of coherence p.

Figure 8 depicts the degree of coherence as a function of the degradation and diffusion coefficients (Fig. 8a, b, respectively). In Fig. 8a, we used $D = 1.0$ and we vary η. The degree of coherence shows a smooth transition from coherent states to incoherent states, and only when $\eta \geq 10$ we observe a completely incoherent state. A similar behavior is found when we vary D and fix η (Fig. 8b), but now the transition is faster and, when $D = 4.2$, incoherent states are already obtained.

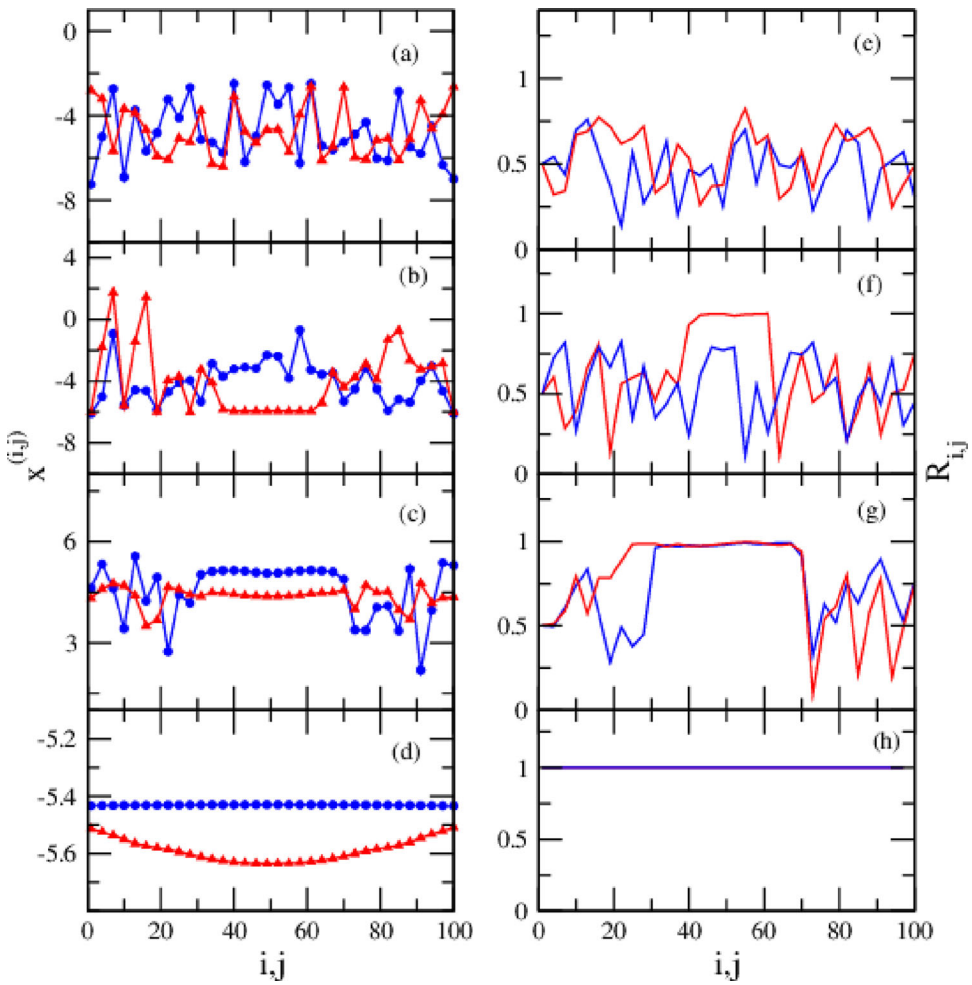


Fig. 6 Snapshot patterns and local order parameters for one-dimensional cross sections of a rectangular lattice of $N = 300$ coupled identical Rössler systems at a fixed time t_F with the following coupling parameters: $D = \eta = 1.0$ and: (a) and (e): $\varepsilon = 0.0$; (b) and (f): $\varepsilon = 0.361$; (c) and (g) $\varepsilon = 0.368$; (d) and (h) $\varepsilon = 0.38$. The remaining parameter values can be found throughout the text

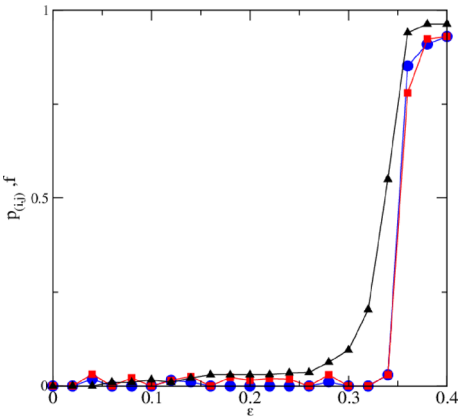


Fig. 7 Degree of coherence $p_{i,j}$ for one-dimensional cross sections of a rectangular lattice of $N = 200$ coupled identical Rössler systems a fixed time t_F with coupling parameters $D = \eta = 1.0$. The black line represents the fraction f characterizing the coherence content of the pattern

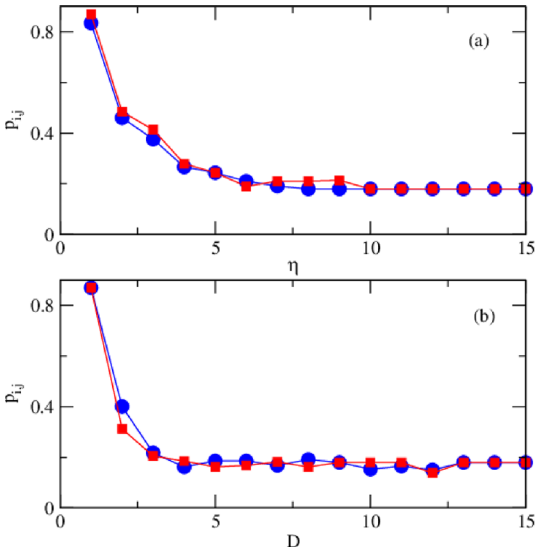


Fig. 8 Degree of coherence $p_{i,j}$ for one-dimensional cross sections of a rectangular lattice of $N = 200$ coupled identical Rössler systems a fixed time t_F with $\varepsilon = 0.375$, as a function of (a) η, for $D = 1.0$; (b) D, for $\eta = 1.0$

For a two-dimensional circle domain of radius, $r = a$ we considered concentric circles of radius $r_i = r_0 + i\,\Delta_r$, where $i = 1, 2, ...N-1$ and $\Delta_r = a/N$. In this way, concentric circles have radius r_0, $r_1 = r_0 + \Delta_r$, $r_2 = r_0 + 2\,\Delta_r$ and so on. Similarly, over each circle we distribute homogeneously the lattice positions by varying the angle according to $\vartheta_j = j\Delta_\vartheta$, where $j = 0, 1, 2, \ldots M-1$ and $\Delta_\vartheta = 2\,\pi/M$. We numerically solved the coupled set of equations (42), with the corresponding equilibrium Green function (33), choosing $a = 1.0$ and $N = M = 10$.

Snapshot patterns, for this geometry, can be observed in Fig. 9. We plot snapshots of slices $\{X_{i,j}\}$ *vs.* i, j, where the i-sites (circle slice) are represented by blue lines and j-sites (radial slice) by red lines at a fixed time t_F. On increasing the coupling parameter, we observed that oscillations start from a totally incoherent state for vanishing coupling (Fig. 9a), then evolve to the emergence of chimera patterns (Fig. 9b, c), until a situation, where the oscillations reach completely coherent states (Fig. 9d, for $\varepsilon = 0.379$).

In Fig. 10, we plot the degree of coherence $p_{(i,j)}$ as a function of the coupling strength for the two-dimensional circle domain, where the blue line refers to the i-sites (circle slice) and the red line to the j-sites (radial slice). We found that the transition from the completely incoherent state to coherent states occurs at $\varepsilon \approx 0.358$, and appears more abrupt in comparison with the similar transition found in the linear domain case. In the same figure, we plot the fraction f (black line), where the transition occurs for $\varepsilon \approx 0.33$.

The inverse transitions for the circle domain, when we used $D = 1.0$ and varied η, are shown in Fig. 11. The degree of coherence shows a smooth transition from coherent states to incoherent states and, only for $\eta \geq 15.0$, we observe a completely incoherent state (Fig. 11a). A similar behavior is found when we vary D and fix η (Fig. 11b). In this case, when $D \geq 15.0$ incoherent states are obtained.

Examples of coherent and incoherent plateaus are shown in the snapshots in Figs. 12 and 13, where we can visualize the results in terms of i and j. For a two-dimensional rectangular domain (Fig. 12a), we plot the snapshots patterns $\{X_{i,j}\}$ *vs.* i, j for particular parameters, where a chimera pattern can be characterized, and then we use the same values to plot the order parameter magnitude (in colorscale) in all sites belonging to a rectangular domain (Fig. 12b). The latter displays a large number of domains with coherent states represented by the yellow pixels,

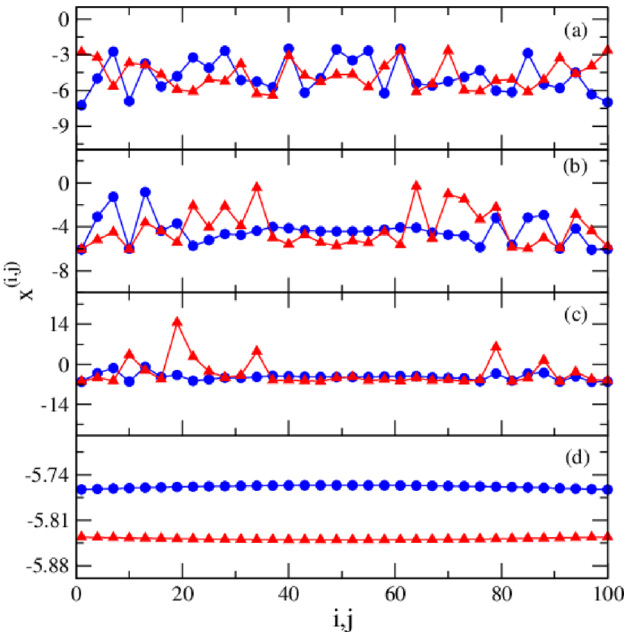


Fig. 9 Snapshot patterns for one-dimensional cross sections of a regular lattice of $N = 200$ coupled identical Rössler systems at a fixed time t_F in a circular domain, with coupling parameters $D = \eta = 1.0$. for (a) $\varepsilon = 0.0$, (b) $\varepsilon = 0.36$, (c) $\varepsilon = 0.367$ and (d) $\varepsilon = 0.379$, where $D = \eta = 1.0$

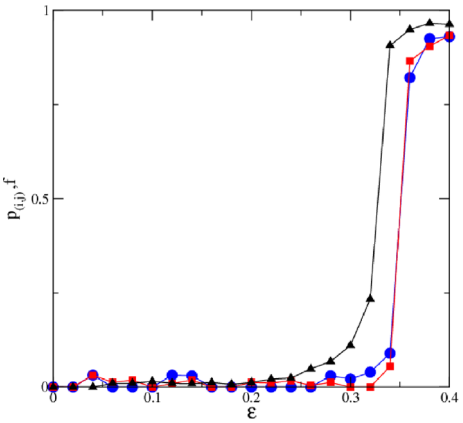


Fig. 10 Degree of coherence p for i (black line and j (red line) for one-dimensional cross sections of a regular lattice of $N = 200$ coupled identical Rössler systems at a fixed time t_F in a circular domain, as a function of the coupling strength, for $D = \eta = 1.0$. The blue line represents the fraction f characterizing the coherence content of the pattern

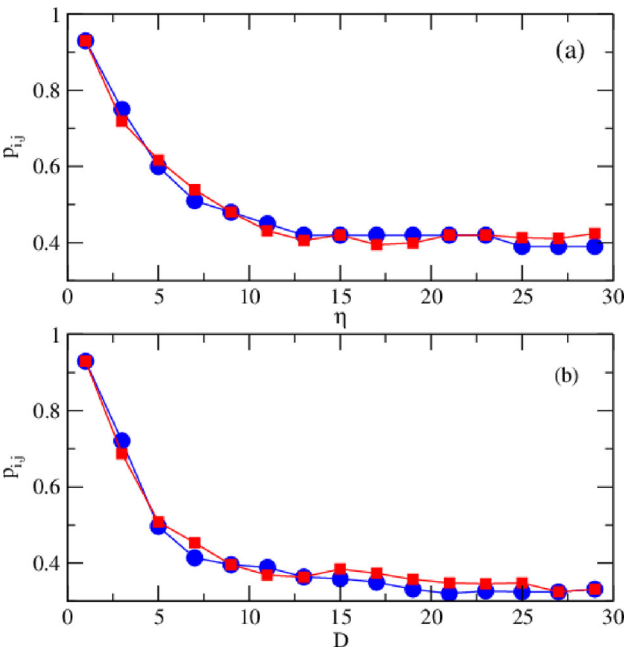


Fig. 11 Degree of coherence p for one-dimensional cross sections of a regular lattice of $N = 200$ coupled identical Rössler systems at a fixed time t_F in a circular domain, for $\varepsilon = 0.37$, as a function of (a) η for $D = 1.0$, (b) D, for $\eta = 1.0$

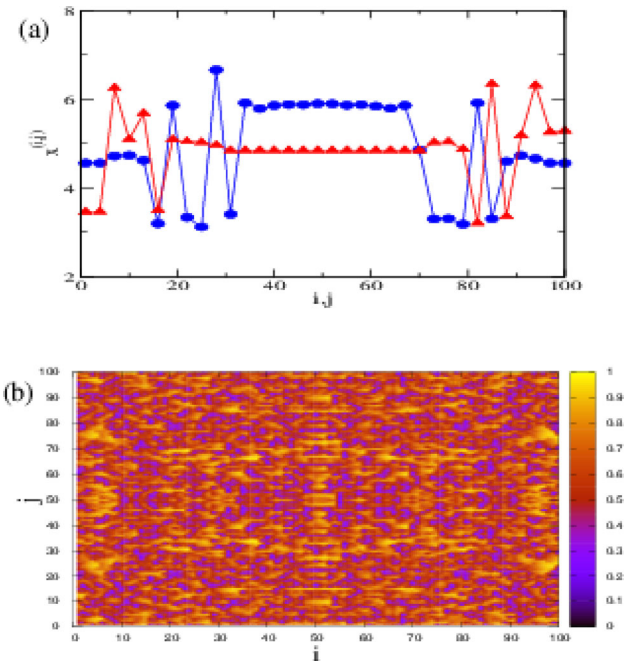


Fig. 12 a Snapshots $\{X_{i,j}\}$ *vs.* i, j for one-dimensional cross sections of a rectangular lattice of $N = 200$ coupled identical Rössler systems a fixed time t_F with coupling parameters $\varepsilon = 0.361$ and $\eta = D = 1.0$. b Order parameter (in colorscale) as a function of i e j for the same parameter values

and the partially incoherent domains are painted by yellow to dark violet pixels. Figure 13a, b shows analogous results for a circular domain.

8 Conclusions

In a variety of problems in physical chemistry and cell biology, the individuals, or cells, undergo some kind of dissipative dynamics leading to a stable limit-cycle as the asymptotic state. The dynamics along this limit-cycle can describe some physico-chemical or biological rhythm, and it can be mathematically described, in a minimal model, by a phase oscillator. We consider the situation in which the oscillator cells are coupled by the diffusion of some substance through the inter-cellular medium. This diffusing chemical is secreted and absorbed according to the cell dynamics, in such a way that the coupling is effectively mediated by the substance.

We proposed a general reaction–diffusion model for this process, where we do not require the diffusion to be infinitely fast, which allows the possibility of diffusion at scales comparable to the oscillator characteristic period. The model can be formulated either in free space (in one, two, and three spatial dimensions) or within closed domains, for which absorbing boundary conditions are assumed. Such boundary conditions, besides being simpler to impose, are actually necessary to avoid saturation of the diffusing substance in the inter-cellular medium. More complicated boundary conditions can be used, though, to tackle specific situations.

Previously, collective phenomena such as phase and frequency synchronization were observed for networks of chemically coupled phase oscillations, modeling a wide variety of systems with physical, chemical, and biological interest. In this work, we extended this analysis to networks of chaotic systems, where a richer spatio-temporal dynamics exists. The collective phenomenon now is the existence of chimera patterns, for which there is a coexistence of coherent and incoherent behavior. To quantify these behaviors, we used a definition of phase and a local parameter introduced by Omel'chenko et al., combined with a definition for the coherence degree based on the lengths of coherence plateaus.

The numerical results, depending on the system parameters, can present three types of behavior. For low coupling values and independent of η and D parameters, incoherent states predominate. For intermediate states of coupling intensity, the chimeras can appear or disappear depending on the variation of the degradation parameter or the diffusion parameter. In the third case, we observed that when we adopt values of the coupling intensity for which there are completely coherent states, it is possible to suppress these states with a combination of values of the diffusion and degradation parameters.

Finally, we can find a transition from incoherent states to fully coherent states depending on the system parameters. In addition, in two-dimensional case studies, the profiles of each geometric slice have different dynamic behavior between them. In other words, for the same set of parameters and the same time instant, the slices can

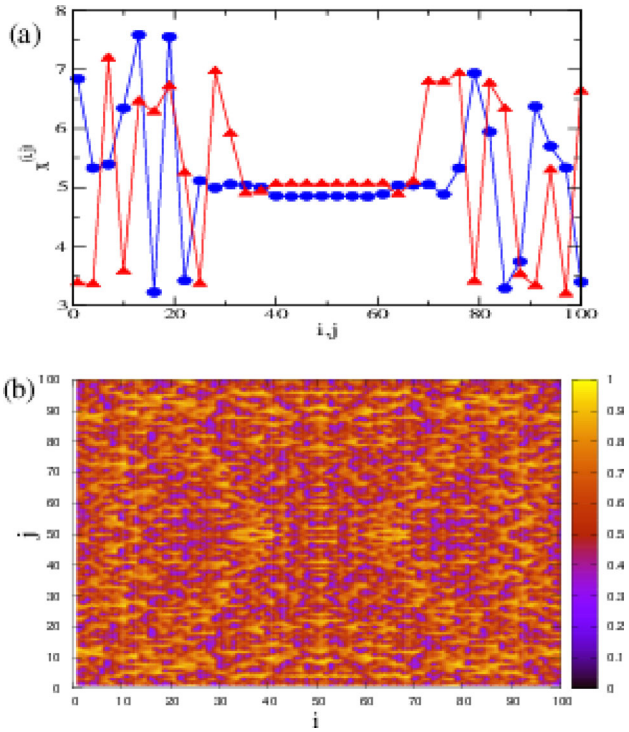


Fig. 13 Snapshots $\{X_{i,j}\}$ *vs.* i, j for one-dimensional cross sections of a rectangular lattice of $N = 200$ coupled identical Rössler systems a fixed time t_F in a circular domain, with coupling parameters $\varepsilon = 0.36$ and $\eta = D = 1.0$. (b) Order parameter (in colorscale) as a function of i e j for the same parameter values

have totally incoherent, chimeric, and totally coherent states, but not identical. In the numerical simulations presented in this work, we used Rössler equations as a paradigm for low-dimensional chaotic systems, but the general features we observed would also be observed for other chaotic systems, albeit for different coupling parameter values.

Acknowledgements One of the authors (R.L.V.) has been partially supported by Conselho Nacional de Desenvolvimento Científico e Tecnológico (CNPq, Brazil) under Grants 403120/2021-7, 443575/2024-0, and 301019/2019-3, and CAPES, grant 88881.895032/2023-01. We acknowledge Pedro Haerter for useful suggestions and discussions.

Data Availability Data used in the production of the figures of the present paper, as well as the C-codes used to produce these data, are available in Zenodo https://doi.org/10.5281/zenodo.17487655

References

1. A. Winfree, *The Geometry of Biological Time* (Springer, 1999)
2. Y. Kuramoto, Prog. Theor. Phys. **94**, 321 (1995)
3. Y. Kuramoto, H. Nakao, Phys. Rev. Lett. **76**, 4352 (1996)
4. Y. Kuramoto, H. Nakao, Physica D **103**, 294 (1997)
5. D. Battogtokh, Prog. Theor. Phys. **102**, 947 (1999)
6. H. Nakao, Chaos **9**, 902 (1999)
7. Y. Kawamura, N. Nakao, Y. Kuramoto, Phys. Rev. E **75**, 036209 (2007)
8. D. Battogtokh, Phys. Lett. A **299**, 558 (2002)
9. H. Sakaguchi, Phys. Rev. E **73**, 031907 (2006)
10. R. L. Viana, A. M. Batista, C. A. S. Batista, J. C. A. de Pontes, F. A. dos S. Silva, and S. R. Lopes, Commun. Nonlinear Sci. Numer. Simulat. **17**, 2924 (2012)
11. F. A. dos S. Silva, S. R. Lopes, R. L. Viana, Commun. Nonlinear Sci. Numer. Simulat. **35**, 37 (2016)
12. C. Liu, D.R. Weaver, S.H. Strogatz, S.M. Reppert, Cell **91**, 855 (1997)
13. C. Liu, S.M. Reppert, Neuron **25**, 123 (2000)
14. C.A.S. Batista, J.D. Szezech Jr., A.M. Batista, E.E.N. Macau, R.L. Viana, Physica A **470**, 236 (2017)
15. R.L. Viana, A.M. Batista, C.A.S. Batista, K.C. Iarosz, Nonlin. Dynam. **87**, 1589 (2017)
16. R.P. Aristides, R.L. Viana, Nonlin. Dynam. **100**, 3759 (2020)
17. P. Haerter, R.L. Viana, Braz. J. Phys. **53**, 114 (2023)
18. O.E. Rössler, Phys. Lett. A **57**, 397 (1976)

19. D.K. Umberger, C. Grebogi, E. Ott, B. Afeyan, Phys. Rev. A **39**, 4835 (1989)
20. J. Crutchfield, K. Kaneko, in Directions in Chaos, B. L. Hao (Ed.) (World Scientific, Singapore) (1987)
21. K. Kaneko, Chaos **2**, 279 (1992)
22. H. Chaté, P. Manneville, Prog. Theor. Phys. **87**, 1 (1992)
23. G. Grégoire, H. Chaté, Phys. Rev. Lett. **92**, 025702 (2004)
24. S.M. Kamil, G.I. Menon, S. Sinha, Chaos **20**, 043123 (2010)
25. D.M. Abrams, S.H. Strogatz, Phys. Rev. Lett. **93**, 174102 (2004)
26. N. Mazouz, G. Flätgen, K. Krischer, Phys. Rev. E **55**, 2260 (1997)
27. K. Wiesenfeld, P. Colet, S. Strogatz, Phys. Rev. Lett. **76**, 404 (1996)
28. L. Larger, B. Penkovsky, Y.L. Maistrenko, Phys. Rev. Lett. **111**, 054103 (2013)
29. A.M. Hagerstrom, T.E. Murphy, R. Roy, P. Hövel, I. Omelchenko, E. Schöll, Nature Phys. **8**, 658 (2012)
30. S. Nkomo, M.R. Tinsley, K. Showalter, Chaos **26**, 094826 (2016)
31. I. Omel'chenko, Y. Maistrenko, P. Hövel, E. Schöll, Phys. Rev. Lett. **106**, 234102 (2011)
32. C.A.S. Batista, R.L. Viana, Physica A **526**, 120869 (2019)
33. C.A.S. Batista, R.L. Viana, Chaos. Solit. Fract. **131**, 109501 (2020)
34. D.G. Duffy, *Green's Functions with Applications* (Chapman & Hall/CRC, Boca Raton, 2001)
35. K. Kaneko, Physica D **34**, 1 (1989)
36. Y. Kuramoto, *Chemical Oscillations, Waves, and Turbulence* (Springer-Verlag, New York, 1984)
37. J.L. Rogers, L.T. Wille, Phys. Rev. E **54**, R2193 (1996)
38. R.L. Viana, A.M. Batista, Chaos. Solit. Fract. **9**, 1931 (1998)

Springer Nature or its licensor (e.g. a society or other partner) holds exclusive rights to this article under a publishing agreement with the author(s) or other rightsholder(s); author self-archiving of the accepted manuscript version of this article is solely governed by the terms of such publishing agreement and applicable law.